



# Preparation and performance of multiwall carbon nanotubes/FeNi<sub>3</sub>/polyaniline composite electrode material for supercapacitors

Jing Huang<sup>1</sup> · Xufeng Song<sup>1</sup> · Chunying He<sup>1</sup> · Zhixin Zhang<sup>1</sup> · Lingxi Qu<sup>1</sup> · Dongyu Zhao<sup>1</sup>

Received: 23 July 2019 / Revised: 17 October 2019 / Accepted: 12 November 2019 / Published online: 9 December 2019  
© Springer-Verlag GmbH Germany, part of Springer Nature 2019

## Abstract

At present, developing a simple, inexpensive, and scalable technology to fabricate an energy storage system remains a challenge. In this study, MWCNTs/FeNi<sub>3</sub>/PANI nanocomposites were prepared by means of in situ polymerization. The morphologies and structure were characterized by the application of various spectral and analytical techniques. When the newly fabricated MWCNTs/FeNi<sub>3</sub>/PANI-20 ternary composite was taken as supercapacitor electrode, the specific capacitance was 398.1 F g<sup>-1</sup> at a current density of 0.5 A g<sup>-1</sup>. In addition, the assembled symmetric supercapacitors displayed not only an excellent cycling property (80.9% capacitance retention after 2000 charge/discharge cycles) but also a remarkable energy and power density (9.1 Wh kg<sup>-1</sup> and 500 W kg<sup>-1</sup>). As revealed by the results, the electrochemical properties of MWCNTs/FeNi<sub>3</sub>/PANI composites can be improved by the synergistic action of various components through the rational selection of electrode materials.

**Keywords** Supercapacitor · Multiwall carbon nanotubes · Polyaniline · Composite

## Introduction

Constantly growing demand for energy is undoubtedly one of the challenges facing the world nowadays [1, 2]. With the continued growth in demand for energy, there is a pressing need to develop an eco-friendly alternative power source. Emerged among various energy storage technologies, supercapacitors have drawn a great deal of attention from both the industry and the scientific communities. In addition, they are used in various applications such as space ship, hybrid electric vehicles, digital cameras, portable electronic devices, backup power, and so on [3, 4]. Moreover, supercapacitors are capable of combining the characteristics of conventional batteries and capacitors, which allows them to not only possess a relative higher energy density and power density but also have a longer cycle life [5–7]. On the basis of the charge storage mechanism, supercapacitors can be split into two categories: (a) electrical double-layer capacitors (EDLCs), which rely on an electrical double-layer generated at the electrode/electrolyte interface for the storage of charge, and

(b) pseudocapacitors (PCs), which store energy through redox reaction, i.e. faradic reaction process.

The most promising design is considered to be the combination of carbonaceous materials, conducting polymers and transition metals. Each component is capable of making a significant contribution to the overall performance of supercapacitors. In carbon materials, we used multiwall carbon nanotubes. Carbon nanotubes are thought to be more advantageous than other carbonaceous materials because they can exhibit high aspect ratio, extraordinary mechanical strength, better charge transfer channels, and greater ease to be intertwined to form durable porous materials [8, 9]. However, the specific capacitance of the original carbon nanotubes is notably low (generally < 100 F g<sup>-1</sup>) [10]. It is noteworthy that the composites derived from using acid-treated nanotubes are capable of higher conductivity, which makes them easier to process without reducing conductivity and it is critical for the effective utilization of their properties. Conducting polymers exhibit large pseudocapacitance and good conductivity, and it has attracted widespread interest as electrode material for supercapacitors [11]. Out of these conducting polymers, polyaniline (PANI) is widely recognized as the most promising electrode material for supercapacitors because of its mechanical flexibility, high conductivity, and chemical stability [12–14]. The main disadvantage of using PANI as supercapacitor electrode is manifested in

✉ Dongyu Zhao  
hacar1201@aliyun.com

<sup>1</sup> School of Chemistry and Materials Science, Heilongjiang University, Harbin, China

its low life cycle, which is attributed to the fact that it experiences swelling and shrinkage when charged and discharged, thus causing mechanical degradation of the electrode [15–18]. However, it could be compensated by the synergy of MWCNTs/PANI composites, within which appropriate functional groups could trigger chemical interaction with the PANI chains. In this case, the specific capacitance and stability of PANI can be significantly improved [19, 20]. On this basis, it is clearly indicated that the combination of carbon materials and pseudocapacitor materials could be effective in boosting the electrochemical performance. Iron-nickel alloy is a sort of material that has been widely applied due to its excellent performance and affordable price. Compared with conventional metals such as Fe, Co, and Ni, FeNi<sub>3</sub> particles display better thermal stability [21–24]. Now, the preparation and research on transition metal-doped conducting polymers remain at the exploratory stage. It is believed that the electrochemical performance is improved due to the effective conductive path achieved by MWCNTs and the synergistic effect of various components in ternary composites. From the study on nanocomposites as electrode materials for supercapacitors, we know the FeNi<sub>3</sub> possess unique magnetic properties in the Fe-Ni alloys [25]. We conducted tests on the composites synthesized in this experiment for their magnetic properties. Meanwhile, the magnetic properties shown by different composites have also been compared, which are expected to be applied in magnetic and sensing nanodevices.

Herein, a two-step method was used to prepare the MWCNTs/FeNi<sub>3</sub>/PANI composites. Firstly, the binary MWCNTs/FeNi<sub>3</sub> was synthesized during the hydrothermal process with MWCNTs, FeSO<sub>4</sub>·7H<sub>2</sub>O, and NiSO<sub>4</sub>·6H<sub>2</sub>O taken as the precursors. As a sort of reducing agent, hydrazine hydrate played a crucial role in the process of binary synthesis. Subsequently, PANI was coated on the MWCNTs/FeNi<sub>3</sub> surface by using in situ polymerization methods. An investigation was conducted into the structure, morphology, magnetic properties, and electrochemical performance of MWCNTs/FeNi<sub>3</sub>/PANI. The results of characterization and performance tests indicated a possibility to maximize the synergistic effects of different components through a sensible selection of functional materials and design of appropriate electrode structures [26–28]. To the best of our knowledge, there is no scientific report on the electrochemical properties displayed by MWCNTs/FeNi<sub>3</sub>/PANI nanocomposites.

## Experimental

### Materials

Multi-walled carbon nanotubes (MWCNTs) were purchased from Shenzhen Nanotech Port Co. Ltd. (Shenzhen, China).

The sample has a diameter of 60–80 nm and a length ranging 5–15 μm based on what is specified by the manufacturer.

Hydrazine hydrate (N<sub>2</sub>H<sub>4</sub>·H<sub>2</sub>O), sodium hydroxide (NaOH), concentrated nitric acid (HNO<sub>3</sub>), concentrated sulfuric acid (H<sub>2</sub>SO<sub>4</sub>), and concentrated hydrochloric acid (HCl) were purchased from Recovery Technology Development Co. Ltd. (Tianjin, China). Ferrous sulfate heptahydrate (FeSO<sub>4</sub>·7H<sub>2</sub>O) and nickel sulfate hexahydrate (NiSO<sub>4</sub>·6H<sub>2</sub>O) were sourced from Ruijin Tianjin Special Chemical Co. Ltd. (Tianjin, China). Cetyltrimethylammonium bromide (CTAB), ammonium persulfate (APS), and aniline (C<sub>6</sub>H<sub>5</sub>NH<sub>2</sub>) were purchased from Tianjin Kemiou Chemical Reagent Co. Ltd. (Tianjin, China). Toluene and ethyl alcohol (C<sub>2</sub>H<sub>5</sub>OH) were purchased from Tianyu Auspicious Technology Co. Ltd. (Beijing, China). All water used in my study was distilled water. All the reagents were applied without further purification in advance.

### Treatment of MWCNTs

In order to develop oxidation groups such as carboxyl group and hydroxyl group on the surface of carbon nanotubes, acid treatment of MWCNTs was required. A mixed acid with a 3:1 volume ratio of concentrated sulfuric acid to concentrated nitric acid was prepared. The MWCNTs was blended with mixed acid at the ratio of 1:100. The MWCNTs weighing 0.6 g was added into the mixed acid solution and stirred at 60 °C for 6 h. The resulting solution was then washed with distilled water until being neutral. MWCNTs were dried in a vacuum oven at 50 °C for 24 h.

### Synthesis of FeNi<sub>3</sub> supported on MWCNTs

A total of 0.34 g FeSO<sub>4</sub>·7H<sub>2</sub>O, 0.96 g NiSO<sub>4</sub>·6H<sub>2</sub>O, and 0.2243 g acidified MWCNTs (the volume fraction of metal compounds to MWCNTs is about 4.66) [29, 30] were gradually added into 30 mL distilled water. In order to disperse the mixture uniformly, ultrasonic treatment was conducted for 40 min. Then, 2 g NaOH was formulated as a solution, and 10 mL hydrazine hydrate as the reducing agent was added into the mixture while being stirred. The mixture was transferred to a Teflon-lined autoclave for reaction at 180 °C for 18 h. Finally, the as-synthesized black product was isolated by filtration, prior to being washed for multiple times with distilled water and 95% of ethanol and dried in a vacuum oven at 50 °C for 24 h.

### Synthesis of the MWCNTs/FeNi<sub>3</sub>/PANI composites

The composites of MWCNTs/FeNi<sub>3</sub>/PANI with varying mass ratios were synthesized by in situ polymerization. The mass ratios of PANI to MWCNTs/FeNi<sub>3</sub> were variable between 10:1, 5:1 and 10:3, and the product signed as MWCNTs/

FeNi<sub>3</sub>/PANI-n, such as MWCNTs/FeNi<sub>3</sub>/PANI-20 composite, indicated that the mass ratio of PANI to MWCNTs/FeNi<sub>3</sub> was 5:1. The preparation process of MWCNTs/FeNi<sub>3</sub>/PANI-20 composite was as follows. A total of 0.1 g MWCNTs/FeNi<sub>3</sub> and 0.5 mL toluene were mixed and sonicated for 40 min. Subsequently, 1.24 g CTAB dissolved in 75 mL distilled water was added to the suspension and treated by ultrasound for 1.5 h. Hydrochloric acid and aniline (0.5 mL) were mixed and then added into the suspension. Then, 2.5 g APS was dissolved into an 11-mL distilled water solution. This APS solution was added drop by drop to the MWCNTs/FeNi<sub>3</sub>-doped aniline solution. Then, the entire solution was reacted in an ice bath for 4 h. When the polymerization process was completed, the entire solution was filtered and washed for multiple times with distilled water and ethanol, prior to being dried at 50 °C for 24 h. Pure PANI was prepared by the same method without the addition of MWCNTs/FeNi<sub>3</sub>. Figure 1 illustrates the preparation process for MWCNTs/FeNi<sub>3</sub>/PANI composites.

## Characterization

X-ray power diffraction (XRD) patterns were recorded using a Rigaku Electric Company diffractometer with Cu-K $\alpha$  radiation. Raman spectra were measured using a Raman spectrometer (Jobin Yvon HR 800) at 632.8 nm. The FTIR spectra of pure PANI, MWCNTs/FeNi<sub>3</sub>, and MWCNTs/FeNi<sub>3</sub>/PANI nanocomposites were performed by using a NEXUS 870 FT-IR (Thermo Nicolet) instrument in the range from 3000 to 500 cm<sup>-1</sup>. An analysis was conducted of the surface morphology of the composites by scanning electron microscopy (SEM: Hitachi S4800) as well as transmission electron microscopy (TEM: JEOL 2100). By using SSLSSX-100 (Evans Analysis Group LLC) X-ray photoelectron spectrometer as well as monochromatic aluminum K $\alpha$  excitation radiation (1253.6 eV), the XPS spectra were determined. An investigation was carried out into the magnetic properties by using a vibrating sample magnetometer (Quantum Design VSM).

## Electrochemical measurements

Electrochemical studies such as cyclic voltammetry (CV), galvanostatic charge/discharge (GCD), and electrochemical

impedance spectroscopy (EIS) were carried out on Chen Hua instrument by using a three-electrode system, where platinum and Hg/HgO electrode were taken as counter and reference electrodes, respectively. The composite was coated onto a nickel foam substrate (1 cm  $\times$  1 cm) and taken as the working electrode. KOH solution (6 M) was taken as electrolyte solution to perform electrochemical measurement. The specific capacitance ( $C$ , F g<sup>-1</sup>) of all composites was calculated from GCD curves by using the following equation:

$$C = (I \times \Delta t) / (m \times \Delta V) \quad (1)$$

where  $I/m$  represents the current density in A g<sup>-1</sup>,  $\Delta V$  is the voltage window, and  $\Delta t$  is the discharge time.

The electrochemical measurements of the assembled symmetric supercapacitor device were performed using a two-electrode system, with the active materials taken as the positive and negative electrodes and polypropylene as a separator. The test was carried out in 6 M KOH electrolyte by using a Land Battery Test System (CT2001A, China). The working electrodes were prepared by the method as mentioned above. All the quality of the electrode materials was controlled about 2 mg cm<sup>-2</sup>. In the two-electrode system, the specific capacitance, energy density, and power density can be calculated from the GCD curves by using the following equations:

$$C_p = (I \times \Delta t) / (m \times \Delta V) \quad (2)$$

$$C_s = 4C_p \quad (3)$$

$$E_p = (C_p \times \Delta V^2) / 7.2 \quad (4)$$

$$P = (3600 \times E_p) / \Delta t \quad (5)$$

where  $C_p$  (F g<sup>-1</sup>),  $C_s$  (F g<sup>-1</sup>),  $E_p$  (Wh kg<sup>-1</sup>), and  $P$  (W kg<sup>-1</sup>) denote the total specific capacitance of the assembled symmetric supercapacitor, the specific capacitance of one electrode, as well as the energy density and power density of the symmetric supercapacitor, respectively.

## Results and discussion

Figure 2 a presents the XRD patterns of MWCNTs, MWCNTs/FeNi<sub>3</sub>, pure PANI, and MWCNTs/FeNi<sub>3</sub>/PANI composites. It can be seen from the figure that the XRD of MWCNTs peak due to the (002) crystalline plane at  $2\theta$  value

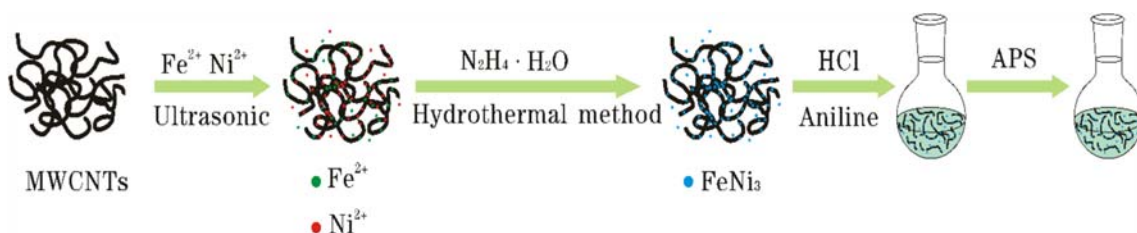


Fig. 1 Preparation process of MWCNTs/FeNi<sub>3</sub>/PANI

of  $26^\circ$ . Figure 2 a shows the XRD pattern of the MWCNTs/FeNi<sub>3</sub> composite, the three characteristic diffraction peaks at  $2\theta = 44^\circ$ ,  $51.3^\circ$ , and  $75.4^\circ$ , which correspond to Miller indices (111), (200), and (220), respectively, and show the presence of fcc FeNi<sub>3</sub> (JCPDS 65-3244). In addition, the peak value of MWCNTs (002) at about  $26^\circ$  still exists. Regarding the pure PANI, the characteristic peaks of PANI at  $2\theta = 15.6^\circ$  (011),  $20.6^\circ$  (020), and  $25.3^\circ$  (200) are clearly observed [31]. As demonstrated by the disappearance of the characteristic peaks for MWCNTs/FeNi<sub>3</sub> in the XRD patterns of the MWCNTs/FeNi<sub>3</sub>/PANI, the MWCNTs/FeNi<sub>3</sub> is fully interacted with PANI molecules and completely covered by PANI particles. Meanwhile, the characteristic peaks of MWCNTs/FeNi<sub>3</sub>/PANI are almost similar to that of pure PANI. It means that PANI on the surface of MWCNTs/FeNi<sub>3</sub> maintains a similar crystalline order to that of pure PANI. As for the nanocomposites, all the peaks of PANI are presented and no new peak is discovered, suggesting no additional crystalline order in the nanocomposites. The XRD results further evidence the success in deriving MWCNTs/FeNi<sub>3</sub>/PANI nanocomposites. Figure 2 b shows XRD patterns of pure PANI and MWCNTs/FeNi<sub>3</sub>/PANI nanocomposites with varying contents of MWCNTs/FeNi<sub>3</sub>. As indicated by the curves, the characteristic peaks corresponding to the ternary composites bear similarity to pure PANI. The peaks in MWCNTs/FeNi<sub>3</sub>/PANI are intense as compared to that of pristine pure PANI, which are attributed to the presence of MWCNTs and FeNi<sub>3</sub>. The diffraction peaks for pure PANI are shown to be weak, suggesting that PANI is in non-crystalline state in the nanocomposites. The presence of non-crystalline PANI weakens the diffraction peaks of FeNi<sub>3</sub> on a continued basis. Upon comparison, MWCNTs/FeNi<sub>3</sub>/PANI-20 is discovered to have a broad crystal peak. Combined with electrochemical characterization, the ratio can lead to a further improvement to crystallinity and conductivity.

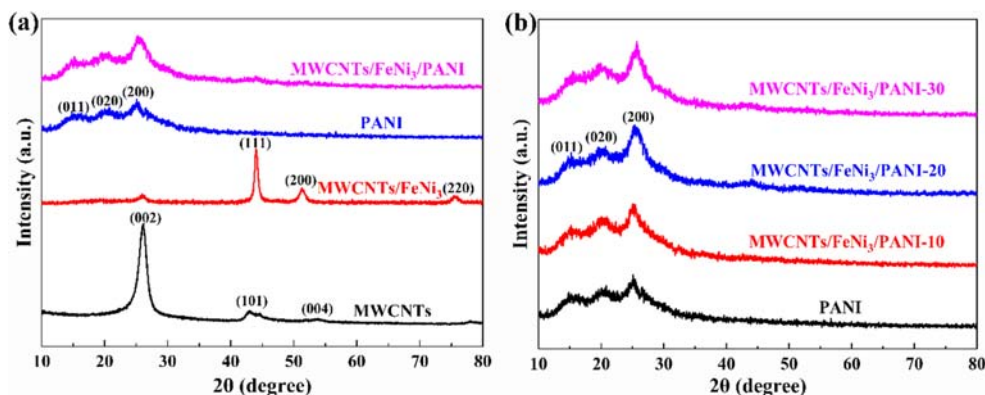
The elemental composition of the MWCNTs/FeNi<sub>3</sub>/PANI-20 composite is analyzed by EDX (energy-dispersive X-ray spectroscopy), as shown in Fig. 3a. The elemental analysis spectrum demonstrates that C, N, O, Fe, and Ni exist in this composite. The Cu signal comes from the supporting film on

the Cu grid. The EDX spectra of all ternary composites are similar, so other samples are not discussed here. Figure 3 b–f shows the element mapping of MWCNTs/FeNi<sub>3</sub>/PANI-20 composite.

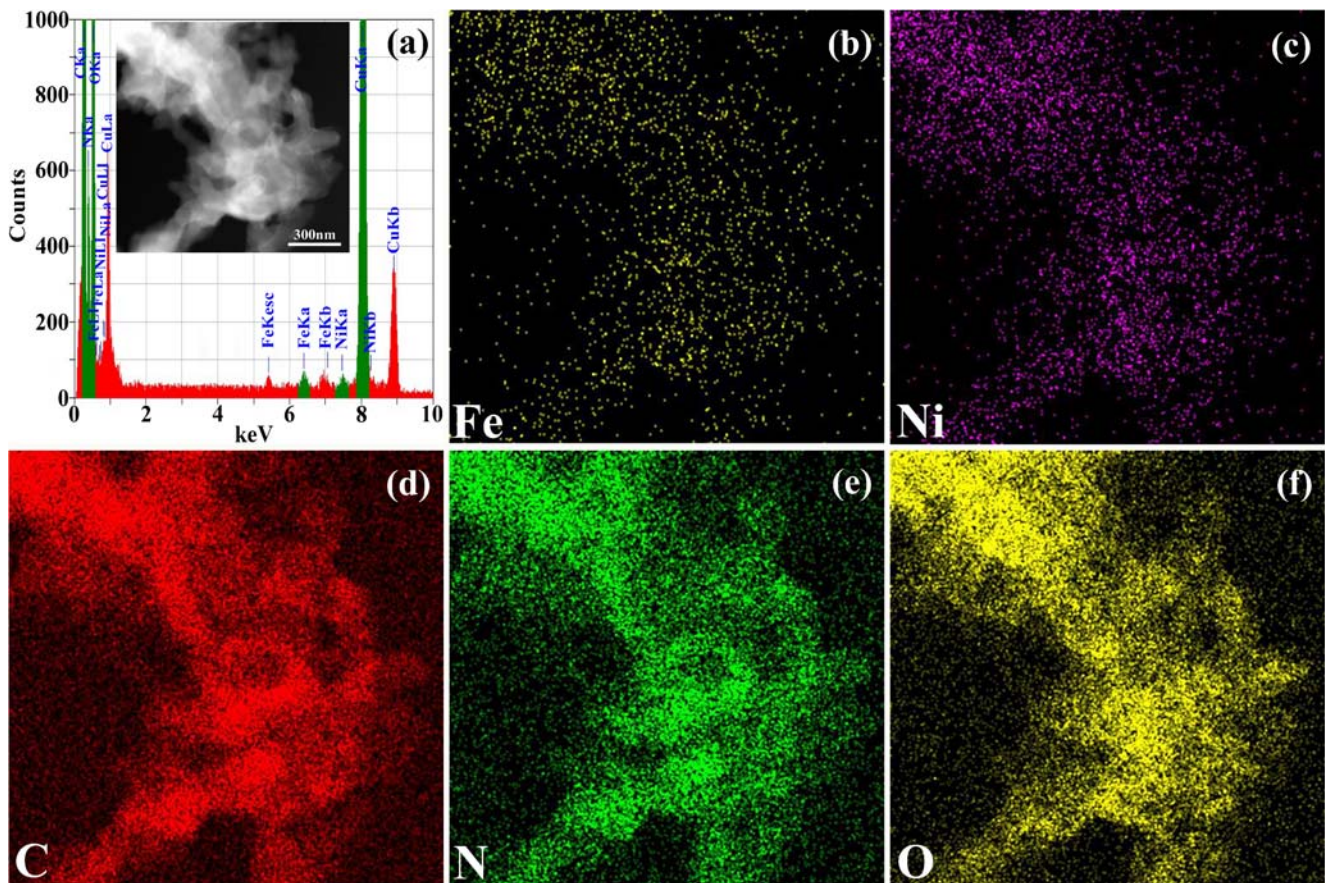
Raman spectra are applied to carry out further investigation into the interaction between samples. The Raman spectra of pure PANI, MWCNTs/FeNi<sub>3</sub>/PANI-10, MWCNTs/FeNi<sub>3</sub>/PANI-20, and MWCNTs/FeNi<sub>3</sub>/PANI-30 are shown in Fig. 4, which reveals pure PANI and ternary composites exhibit two typical bands, including strong D band and weak G band. Normally, the D band ( $1330\text{ cm}^{-1}$ ) is associated with the structural defect, whereas the G band ( $1560\text{ cm}^{-1}$ ) represents the in-plane vibration of  $sp^2$  carbon atoms [32]. The ratios of D to G bands ( $I_D/I_G$ ) reflect the extent of structural defect. The  $I_D/I_G$  ratios of pure PANI, MWCNTs/FeNi<sub>3</sub>/PANI-10, MWCNTs/FeNi<sub>3</sub>/PANI-20, and MWCNTs/FeNi<sub>3</sub>/PANI-30 are 1.21, 1.24, 1.43, and 1.52, respectively. Among them, the defect density of ternary composites gradually rose with the increasing in the amount of MWCNTs/FeNi<sub>3</sub> [33]. Hereby, the peak of the ternary composites becomes sharper than pure PANI, which is primarily attributed to the  $\pi$ - $\pi^*$  electron interaction between PANI and MWCNTs [34].

Figure 5 clearly demonstrates the FT-IR spectra of PANI, MWCNTs/FeNi<sub>3</sub>, and MWCNTs/FeNi<sub>3</sub>/PANI-20 nanocomposites. The FTIR peaks of pure PANI exhibit quinoid and benzenoid stretching vibration around  $1571\text{ cm}^{-1}$  and  $1490\text{ cm}^{-1}$ , respectively. In MWCNTs/FeNi<sub>3</sub>/PANI-20, these two peaks shift to  $1569\text{ cm}^{-1}$  and  $1485\text{ cm}^{-1}$ , indicating that the proton-induced spin unpairing mechanism leads to a higher charge delocalization [35]. The C–N stretching vibration at  $1296\text{ cm}^{-1}$  of pure PANI is observed to shift in ternary composite to  $1294\text{ cm}^{-1}$ . The peak at  $1136\text{ cm}^{-1}$  of pure PANI corresponds to the N = Q = N (Q denotes quinoid) stretching, shifting to  $1128\text{ cm}^{-1}$  in the MWCNTs/FeNi<sub>3</sub>/PANI-20 composite [36]. The peak at  $798\text{ cm}^{-1}$  for pure PANI and  $796\text{ cm}^{-1}$  for the MWCNTs/FeNi<sub>3</sub>/PANI-20 composite indicates the C–H out of plane bending vibration. All pure PANI characteristic peaks are exhibited in MWCNTs/FeNi<sub>3</sub>/PANI-20 composite with a shift of peaks. These shifting peaks indicate the structural changes in the polymer backbone during

**Fig. 2** a XRD patterns of MWCNTs, MWCNTs/FeNi<sub>3</sub>, PANI, and MWCNTs/FeNi<sub>3</sub>/PANI. b XRD patterns of PANI, MWCNTs/FeNi<sub>3</sub>/PANI-10, MWCNTs/FeNi<sub>3</sub>/PANI-20, and MWCNTs/FeNi<sub>3</sub>/PANI-30







**Fig. 3** a EDX spectrum of MWCNTs/FeNi<sub>3</sub>/PANI-20. b–f Elemental maps of Fe, Ni, C, N, and O in MWCNTs/FeNi<sub>3</sub>/PANI-20. All data comes from the selected area in a

doping process and also signifies the interaction between MWCNTs/FeNi<sub>3</sub> and PANI.

An analysis is conducted of the surface composition of MWCNTs/FeNi<sub>3</sub> composite with X-ray photoelectron spectroscopy. Figure 6 a shows the survey spectrum of

MWCNTs/FeNi<sub>3</sub>. The characteristic peaks of C1s, N1s, O1s, Fe2p, and Ni2p elements can be easily identified among the full spectrum. The mass concentrations of the elements present in the MWCNTs/FeNi<sub>3</sub> composite are 38.56%, 2.64%, 20.36%, 9.33% and 29.11% for C, N, O, Fe, and Ni, respectively. No other impurities are introduced. As for MWCNTs/

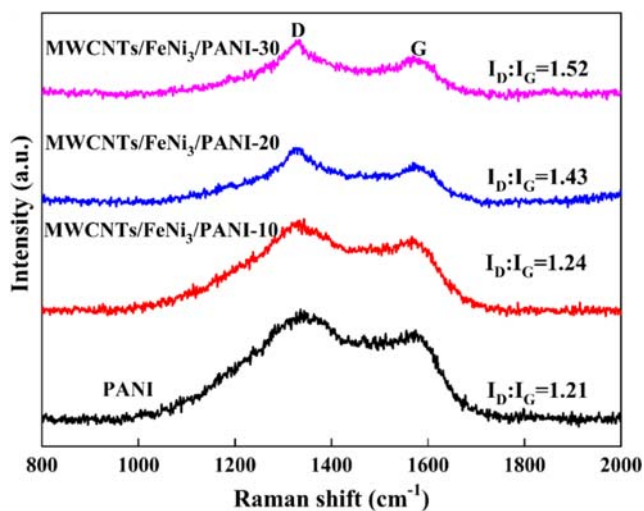


**Fig. 4** Raman spectra of PANI, MWCNTs/FeNi<sub>3</sub>/PANI-10, MWCNTs/FeNi<sub>3</sub>/PANI-20, and MWCNTs/FeNi<sub>3</sub>/PANI-30

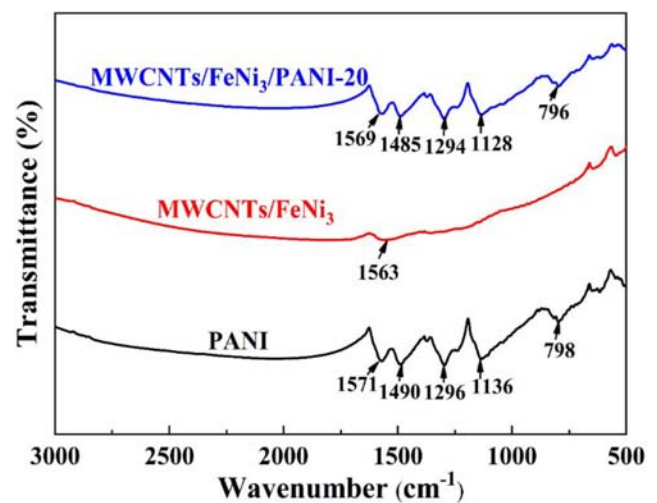
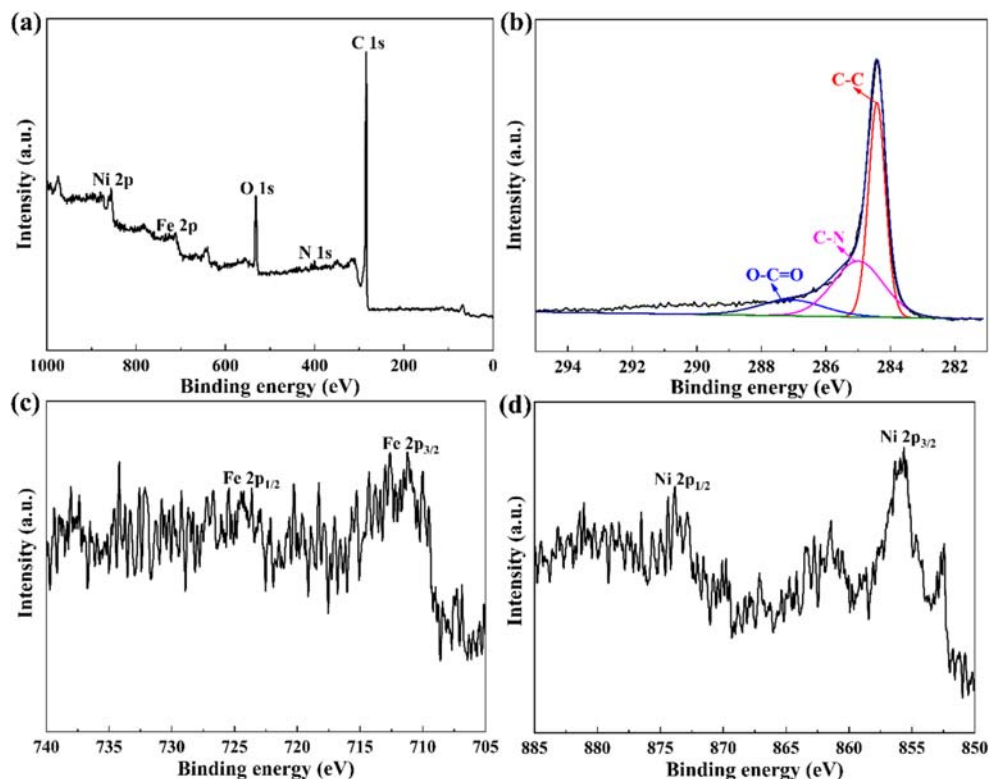


**Fig. 5** FT-IR spectra of PANI, MWCNTs/FeNi<sub>3</sub>, and MWCNTs/FeNi<sub>3</sub>/PANI-20

**Fig. 6** XPS spectra of **a** survey spectrum of MWCNTs/FeNi<sub>3</sub>, **b** C1s XPS spectrum of MWCNTs/FeNi<sub>3</sub>, **c** Fe2p, and **d** Ni2p XPS spectra of the as-prepared MWCNTs/FeNi<sub>3</sub>



FeNi<sub>3</sub>, the high-resolution C1s spectrum (Fig. 6b) is divided into three components corresponding to carbon atoms in different functional groups: C–C (sp<sup>2</sup> carbon), C–N, and O–C=O, and the binding energies are 284.4 eV, 285 eV, and 288.1 eV, respectively. Figure 6 c, d represents the XPS spectra of Fe2p and Ni2p, respectively. The Fe2p level with binding energy peaks of 711.1 and 724.5 eV are attributed to Fe2p<sub>3/2</sub> and Fe2p<sub>1/2</sub>, respectively. The binding energy of core level at 855.6 eV and 873.8 eV are Ni2p<sub>3/2</sub> and Ni2p<sub>1/2</sub>, respectively.

As revealed by the SEM image of a typical MWCNTs/FeNi<sub>3</sub> sample, the FeNi<sub>3</sub> nanoparticles are uniformly attached to MWCNTs. Figure 7 b presents TEM image of MWCNTs/FeNi<sub>3</sub> with a magnification higher than that of Fig. 7a. The morphologies of nanoparticles and MWCNTs are clearly observed and the FeNi<sub>3</sub> particles show a sphere appearance. The deposition of nanoparticles uniformly attached to MWCNTs is contributed to by the functional sites on the surface of MWCNTs which are developed as the result of the mixed acid oxidation treatment. Figure 7 c–f shows the SEM images of pure PANI and MWCNTs/FeNi<sub>3</sub>/PANI composites with varying contents of MWCNTs/FeNi<sub>3</sub>. Figure 7 c presents the SEM image of pure PANI. Figure 7 d–f indicates the formation of a virgulate-like structure, suggesting that the surface of MWCNTs/FeNi<sub>3</sub> is completely covered by PANI. This morphology is capable of improving the electrochemical performance of the ternary composites. From these images, it can be judged that the presence of MWCNTs in the reaction system exerts a substantial influence on the morphology of PANI. In addition, MWCNTs can be

applied as a conductive material and a conductive network could be constructed. The uniform MWCNTs, coating ensures a more desirable synergistic effect, thus assisting the composites to exhibit superior electrode material properties.

In order to validate the electrochemical performance of pure PANI and MWCNTs/FeNi<sub>3</sub>/PANI composites, CV analysis is performed. The CV displays 0–0.8 v in the potential window. Figure 8 a shows the CV curves of pure PANI, MWCNTs/FeNi<sub>3</sub>/PANI-10, MWCNTs/FeNi<sub>3</sub>/PANI-20, and MWCNTs/FeNi<sub>3</sub>/PANI-30 at a scan rate of 200 mV s<sup>-1</sup>. The CV curves exhibit apparent redox peaks, which are largely attributed to the leucoemeraldine/emeraldine and emeraldine/ pernigraniline redox reactions of PANI. As revealed by the figure, pure PANI and ternary composites have the identical type of peaks, except that some shifting occurs. This peak shift results from the electrode resistance. Generally speaking, the specific capacitance is proportional to the area of their CV curve. As shown by the figure, the CV area of all ternary composites is larger than pure PANI, which suggests the ternary composites exhibit more pseudocapacitance when MWCNTs/FeNi<sub>3</sub> is added. Moreover, the CV area of MWCNTs/FeNi<sub>3</sub>/PANI-20 composite is found to be larger than that of other ternary composites. The results show that the synergistic effects of the MWCNTs, FeNi<sub>3</sub>, and PANI result in better contact among all the components. Figure 8 b presents the CV curves of MWCNTs/FeNi<sub>3</sub>/PANI-20 ternary composite at varying scanning rates. The redox current increases with the increasing scan rates and shows an excellent



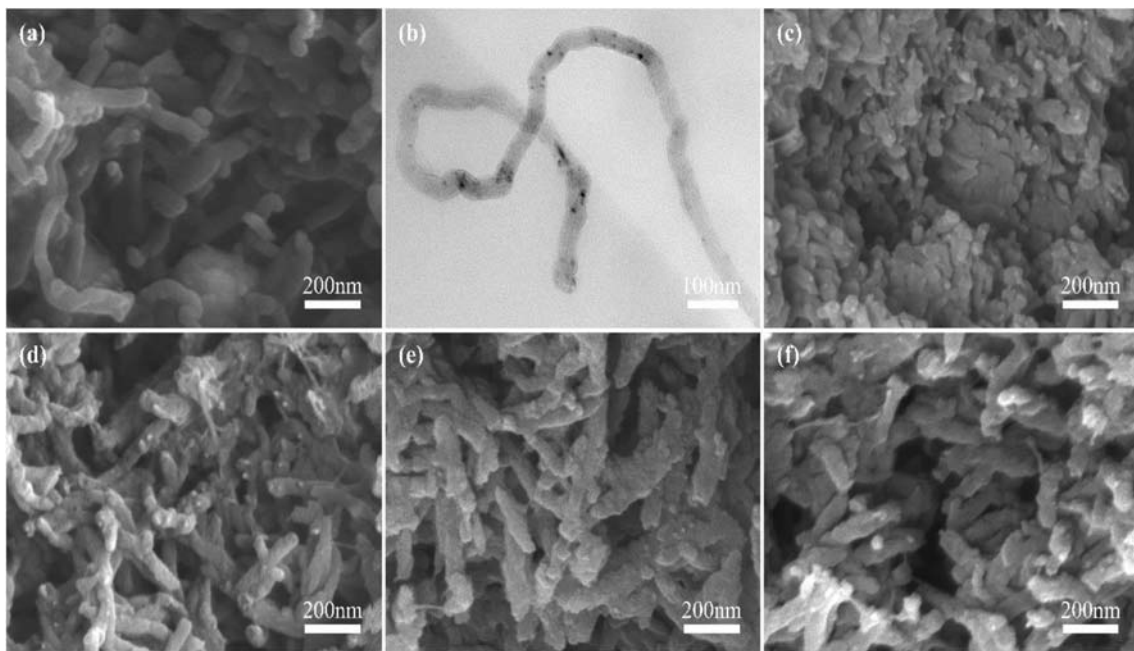


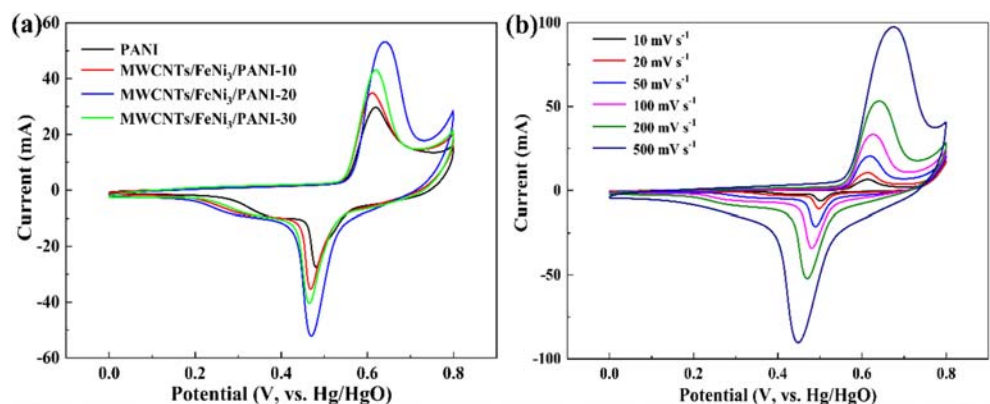
**Fig. 7** **a** SEM image and **b** TEM image of MWCNTs/FeNi<sub>3</sub>. SEM images of **c** PANI, **d** MWCNTs/FeNi<sub>3</sub>/PANI-10, **e** MWCNTs/FeNi<sub>3</sub>/PANI-20, and **f** MWCNTs/FeNi<sub>3</sub>/PANI-30

rate capability. The overall shape of MWCNTs/FeNi<sub>3</sub>/PANI-20 composite is similar at different scanning rates, suggesting that the electrode material has a desirable reversibility. Based on this, the electrochemical performance of the ternary composite is considered as ideal.

To ensure a better evaluation of the electrochemical performance of the electrode materials, the galvanostatic charge/discharge method is applied. Figure 9 a presents the galvanostatic charge/discharge curves of pure PANI, MWCNTs/FeNi<sub>3</sub>/PANI-10, MWCNTs/FeNi<sub>3</sub>/PANI-20, and MWCNTs/FeNi<sub>3</sub>/PANI-30 composites at 1 A g<sup>-1</sup> current density. With the use of Eq. (1), the specific capacitance values of pure PANI, MWCNTs/FeNi<sub>3</sub>/PANI-10, MWCNTs/FeNi<sub>3</sub>/PANI-20, and MWCNTs/FeNi<sub>3</sub>/PANI-30 at 1 A g<sup>-1</sup> current density are calculated to be 122.5, 246.3, 356.2, and 321.8 F g<sup>-1</sup>, respectively. As demonstrated by the data, the specific capacitance of the ternary composites is higher than that of pure

PANI, indicating that the synergistic effect between MWCNTs/FeNi<sub>3</sub> and PANI are crucial to improving the specific capacitance performance. Meanwhile, the specific capacitance of the MWCNTs/FeNi<sub>3</sub>/PANI-20 is higher than that of other ternary composites! the best performance is achieved and conforming to the CV results. Figure 9 b shows the GCD curves of the MWCNTs/FeNi<sub>3</sub>/PANI-20 at the current densities of 0.5, 1, 2, 3, 5, and 10 A g<sup>-1</sup>. As the current density is raised, the discharge time of the ternary composites is reduced, causing the specific capacitance value to be lower. The specific capacitance values of the MWCNTs/FeNi<sub>3</sub>/PANI-20 nanocomposite is 398.1, 356.2, 295.0, 243.8, 212.5, and 178.7 F g<sup>-1</sup> at the current density of 0.5, 1, 2, 3, 5, and 10 A g<sup>-1</sup>, respectively. The specific capacitance changes with current density as shown in Fig. 9c, which suggests the composite is capable of excellent capacitive behavior and charge/discharge performance. A comparison is performed between

**Fig. 8** **a** CV curves of PANI, MWCNTs/FeNi<sub>3</sub>/PANI-10, MWCNTs/FeNi<sub>3</sub>/PANI-20, and MWCNTs/FeNi<sub>3</sub>/PANI-30 at 200 mV s<sup>-1</sup>. **b** CV curves of MWCNTs/FeNi<sub>3</sub>/PANI-20 nanocomposite at different scanning rates. All data are obtained under the three-electrode testing system



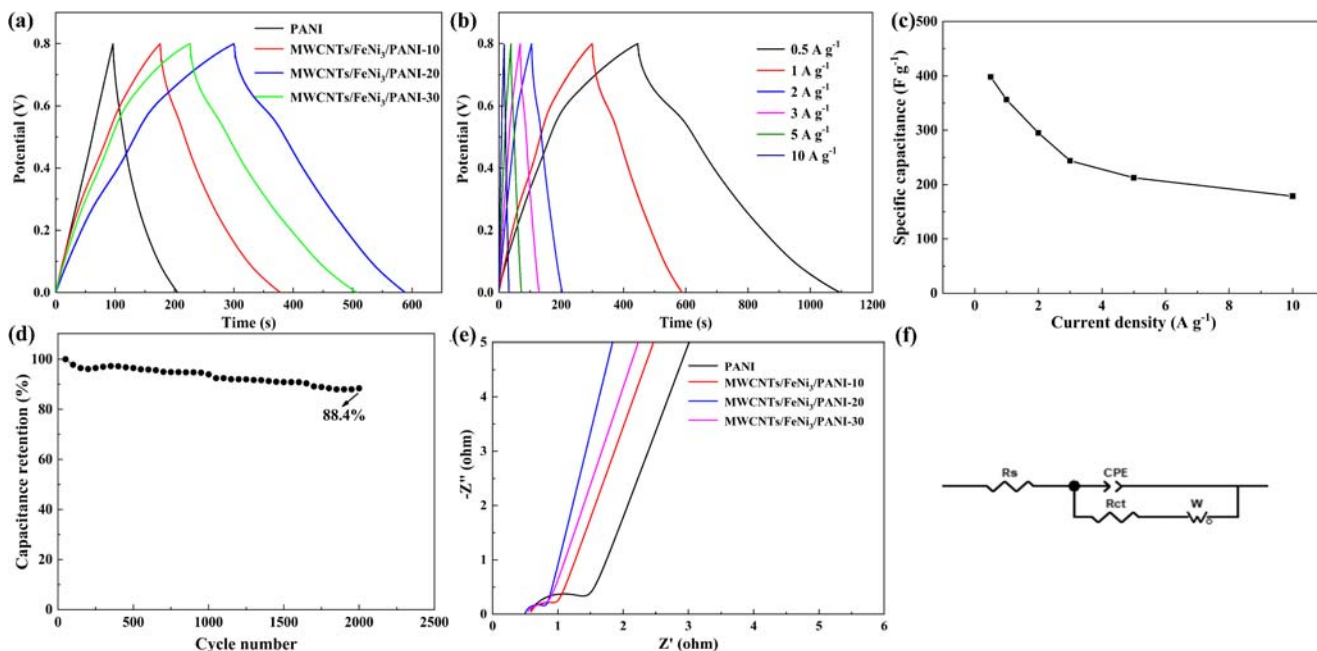


**Fig. 9** **a** GCD curves of PANI, MWCNTs/FeNi<sub>3</sub>/PANI-10, MWCNTs/FeNi<sub>3</sub>/PANI-20 and MWCNTs/FeNi<sub>3</sub>/PANI-30 at 1 A g<sup>-1</sup>. **b** GCD curves of MWCNTs/FeNi<sub>3</sub>/PANI-20 at different current densities. **c** Specific capacitance of MWCNTs/FeNi<sub>3</sub>/PANI-20 with different current densities. **d** Cycle test of the MWCNTs/FeNi<sub>3</sub>/PANI-20 electrode at

50 mV s<sup>-1</sup>. **e** EIS curves of PANI, MWCNTs/FeNi<sub>3</sub>/PANI-10, MWCNTs/FeNi<sub>3</sub>/PANI-20, and MWCNTs/FeNi<sub>3</sub>/PANI-30. **f** Equivalent circuit used for fitting the Nyquist plot. All data are obtained under the three-electrode testing system

the specific capacitance values calculated from the GCD curves and the electrochemical performance of PANI-based materials reported previously, as shown in Table 1.

Regarding supercapacitors, the cyclic stability of electrode materials is known as a significant part of its practical application. Figure 9 d shows the graph of cycle times of the MWCNTs/FeNi<sub>3</sub>/PANI-20 composite at a scanning rate of 50 mV s<sup>-1</sup>. The results reveal a sharp decline in the specific capacitance of the composite during the initial cycles; however, this phenomenon does not occur with the increasing of cycle times. The fast-paced decrease in the initial specific

capacitance can be attributed to the degradation of PANI, which results from swelling and shrinkage of the polymers during the charge/discharge process. This leads to the deterioration in cycle stability. Owing to the combination of MWCNTs/FeNi<sub>3</sub> and PANI, the mechanical strength of the composite is improved, and it is conducive to enhance the electrochemical stability. After 2000 cycles, the specific capacitance retention of the MWCNTs/FeNi<sub>3</sub>/PANI-20 composite is 88.4%, suggesting a long-term electrochemical stability.

EIS spectroscopy is used to assist with the analysis of the resistance information about electrode materials. The

**Table 1** Comparison of the specific capacitance of the reported PANI-based electrodes and the similar work

Materials	Electrolyte	Current density	Capacitance (F g <sup>-1</sup> )	Ref.
MWCNTs/FeNi <sub>3</sub> /PANI-20	6 M KOH	0.5 A g <sup>-1</sup>	398.1 F g <sup>-1</sup>	This work
Fe <sub>3</sub> O <sub>4</sub> /CNTs/PANI-8	1 M KOH	0.5 A g <sup>-1</sup>	260 F g <sup>-1</sup>	[37]
PANI-MWCNTs-TiO <sub>2</sub>	1 M H <sub>2</sub> SO <sub>4</sub>	0.4 A g <sup>-1</sup>	270 F g <sup>-1</sup>	[38]
PANI/TCN	1 M H <sub>2</sub> SO <sub>4</sub>	0.5 A g <sup>-1</sup>	373.5 F g <sup>-1</sup>	[39]
RGO/UCNTs/PANI	1 M H <sub>2</sub> SO <sub>4</sub>	1 A g <sup>-1</sup>	359.3 F g <sup>-1</sup>	[33]
CNT-PANI	0.5 M H <sub>2</sub> SO <sub>4</sub>	0.5 A g <sup>-1</sup>	368.4 F g <sup>-1</sup>	[40]
PANI/MnO <sub>2</sub>	1 M Na <sub>2</sub> SO <sub>4</sub>	0.35 A g <sup>-1</sup>	320 F g <sup>-1</sup>	[41]
PANI/MnO <sub>2</sub> -MWCNTs	0.5 M Na <sub>2</sub> SO <sub>4</sub>	0.2 A g <sup>-1</sup>	350 F g <sup>-1</sup>	[42]
AC/MnO <sub>2</sub> /PANI	1 M Na <sub>2</sub> SO <sub>4</sub>	1 A g <sup>-1</sup>	245 F g <sup>-1</sup>	[43]
CNFs/CNTs/PANI	1 M H <sub>2</sub> SO <sub>4</sub>	1 A g <sup>-1</sup>	315 F g <sup>-1</sup>	[44]



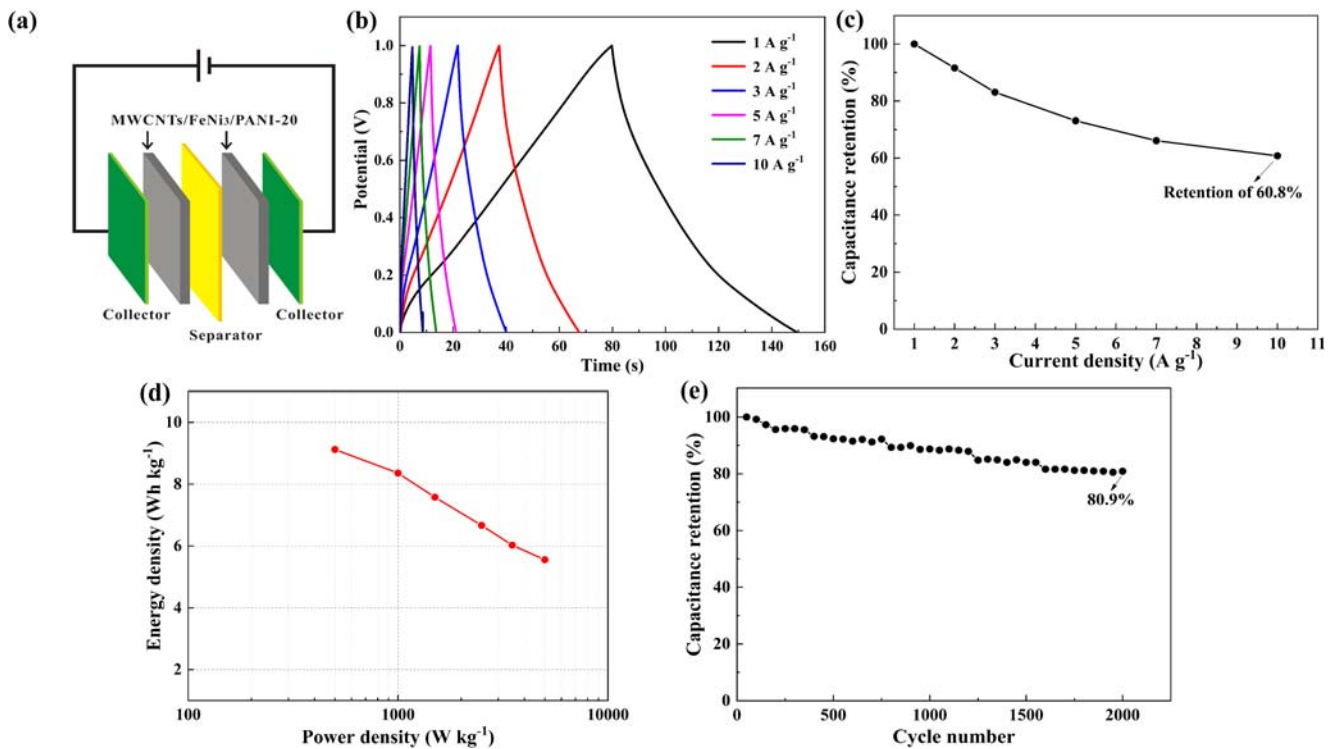


**Fig. 10** a Schematic illustration of the assembled structure of the MWCNTs/FeNi<sub>3</sub>/PANI-20//MWCNTs/FeNi<sub>3</sub>/PANI-20. b GCD curves of MWCNTs/FeNi<sub>3</sub>/PANI-20//MWCNTs/FeNi<sub>3</sub>/PANI-20 at different current densities. c Rate capability at different current densities. d

Ragone plot of the MWCNTs/FeNi<sub>3</sub>/PANI-20//MWCNTs/FeNi<sub>3</sub>/PANI-20 supercapacitor. e Cycling performance of the MWCNTs/FeNi<sub>3</sub>/PANI-20//MWCNTs/FeNi<sub>3</sub>/PANI-20 supercapacitor at a current density of 5 A g<sup>-1</sup>. All data are obtained under the two-electrode testing system

impedance measurements are performed in the frequency range of 0.01–1 × 10<sup>5</sup> Hz. For the composites, the Nyquist plot is represented in Fig. 9e after fitting with an equivalent electrical circuit, with the circuit illustrated in Fig. 9f. The Nyquist plot consists of two parts, including a semicircle in the high-frequency region and a straight line in the low-frequency region. The semicircle diameter denotes the charge

transfer resistance ( $R_{ct}$ ) of the composites. In accordance with the figure, a conclusion can be drawn that the MWCNTs/FeNi<sub>3</sub>/PANI-20 composite is the smallest semicircle diameter. A smaller diameter of the semicircle leads to a better charge transfer performance that can be achieved with the increase in the available surface area. According to the fitted Nyquist plot, the charge transfer resistances of PANI, MWCNTs/FeNi<sub>3</sub>/PANI-10, MWCNTs/FeNi<sub>3</sub>/PANI-20, and MWCNTs/FeNi<sub>3</sub>/PANI-30 are 0.97 Ω, 0.50 Ω, 0.31 Ω, and 0.39 Ω, respectively. The intuitive  $R_{ct}$  values illustrate the advantages of MWCNTs/FeNi<sub>3</sub>/PANI-20. Moreover, the solution resistance ( $R_s$ ) is obtained by the intercepts of the curves with the X-axis. The solution resistances of 0.57 Ω, 0.54 Ω, 0.46 Ω, and 0.51 Ω are obtained for PANI, MWCNTs/FeNi<sub>3</sub>/PANI-10, MWCNTs/FeNi<sub>3</sub>/PANI-20, and MWCNTs/FeNi<sub>3</sub>/PANI-30 nanocomposites, respectively. The lowest  $R_s$  value of MWCNTs/FeNi<sub>3</sub>/PANI-20 improves its superior conductivity and specific capacitance. The presence of a more vertical line indicates that the composite has better electrochemical behavior. At low-frequency region, the slope of MWCNTs/FeNi<sub>3</sub>/PANI-20 is larger than that of other composites, which suggests the excellent capacitance behavior of the MWCNTs/FeNi<sub>3</sub>/PANI-20 composite. The time constant is another important indicator for the evaluation of the charge/discharge time of supercapacitors. Composites with low time constant

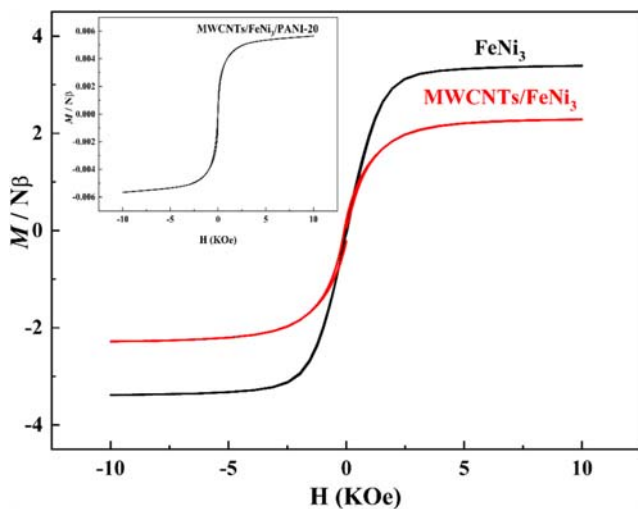


**Fig. 11** Magnetization curves of FeNi<sub>3</sub>, MWCNTs/FeNi<sub>3</sub>, and MWCNTs/FeNi<sub>3</sub>/PANI-20

is the first choice for supercapacitor electrode materials [38, 45]. The obtained time constant of MWCNTs/FeNi<sub>3</sub>/PANI-20 is 2.84 s, which is lower than PANI (5.56 s), MWCNTs/FeNi<sub>3</sub>/PANI-10 (4.19 s), and MWCNTs/FeNi<sub>3</sub>/PANI-30 (3.43 s), indicating that MWCNTs/FeNi<sub>3</sub>/PANI-20 exhibits better fast-charge/discharge properties. Therefore, it concludes that the addition of MWCNTs/FeNi<sub>3</sub> can effectively improve the electrochemical performance of PANI.

To conduct an in-depth investigation into the electrochemical performance of MWCNTs/FeNi<sub>3</sub>/PANI-20 composite, a symmetric supercapacitor is assembled and tested by the two-electrode system in 6 M KOH electrolyte (Fig. 10a). Figure 10 b shows the GCD curves of the MWCNTs/FeNi<sub>3</sub>/PANI-20//MWCNTs/FeNi<sub>3</sub>/PANI-20 at different current densities. According to these GCD curves, the total specific capacitance values in the two-electrode setup can be calculated by the Eq. (2) as 65.7 F g<sup>-1</sup> (1 A g<sup>-1</sup>), 60.2 F g<sup>-1</sup> (2 A g<sup>-1</sup>), 54.6 F g<sup>-1</sup> (3 A g<sup>-1</sup>), 48 F g<sup>-1</sup> (5 A g<sup>-1</sup>), 43.4 F g<sup>-1</sup> (7 A g<sup>-1</sup>), and 40 F g<sup>-1</sup> (10 A g<sup>-1</sup>), respectively. When the current density increases from 1 to 10 A g<sup>-1</sup>, the capacitance is shown to remain 60.8% of the initial value (Fig. 10c), indicating the composite has excellent rate capability. Figure 10 d depicts the corresponding Ragone plot of the symmetric supercapacitor at different current densities. When the power density is 500 W kg<sup>-1</sup>, the energy density is up to 9.1 Wh kg<sup>-1</sup>, and when the energy density drops to 5.6 Wh kg<sup>-1</sup>, the power density is 5004 W h kg<sup>-1</sup>. Concerning the comprehensive performance of power and energy densities, the composite is found to be superior to the previous results as reported, for instance RGO/UCNTs/PANI//RGO/UCNTs/PANI SC (6.6 Wh kg<sup>-1</sup> at 1957.7 W kg<sup>-1</sup>) [33], CNFs/PANI//CNFs/PANI SC (4.5 Wh kg<sup>-1</sup> at 103 W kg<sup>-1</sup>) [46], TCPs/PANI//TCPs/PANI SC (5.8 Wh kg<sup>-1</sup> at 530 W kg<sup>-1</sup>) [47], etc. Figure 10 e shows the capacitance retention of composite at a constant current density of 5 A g<sup>-1</sup> with 2000 charge/discharge cycles. After continuous charging-discharging cycles, the capacitance retention of the ternary composite reaches about 80.9%, further demonstrating its high rate performance and excellent long-term stability.

The magnetic properties of FeNi<sub>3</sub>, MWCNTs/FeNi<sub>3</sub>, and MWCNTs/FeNi<sub>3</sub>/PANI-20 nanocomposites are characterized by vibrating sample magnetometer (VSM) at room temperature, as shown in Fig. 11. Because of FeNi<sub>3</sub> nanoalloy possesses typical soft magnetic characteristics, its magnetic hysteresis loop resembles S-like. According to the M-H curves, the nanocomposites containing FeNi<sub>3</sub> particles demonstrate ferromagnetic behavior. The saturation magnetization values of FeNi<sub>3</sub>, MWCNTs/FeNi<sub>3</sub>, and MWCNTs/FeNi<sub>3</sub>/PANI-20 are 3.39, 2.29, and 0.0056 Nβ, respectively. Therefore, this study confirms that the synthesized binary and ternary composites continue to possess acceptable magnetic properties, which means that nanocomposites are capable of quick response to the external magnetic field and have a certain degree of dispersion.

## Conclusions

In summary, MWCNTs/FeNi<sub>3</sub>/PANI nanocomposites had been synthesized by in situ polymerization method. Due to the synergistic effect of the three components, the ternary composites exhibit superior electrochemical performance to pure PANI. Spectroscopic results revealed the interaction among MWCNTs, FeNi<sub>3</sub> and PANI. The uniform coating of PANI on the surface of MWCNTs/FeNi<sub>3</sub> was analyzed by SEM and TEM. VSM demonstrated that different nanocomposites remain in possession of certain magnetic properties. The MWCNTs/FeNi<sub>3</sub>/PANI-20 nanocomposite achieved a specific capacitance of 398.1 F g<sup>-1</sup> when the current density was 0.5 A g<sup>-1</sup>. The ternary composite maintained 88.4% specific capacitance following 2000 charge/discharge cycles. Meanwhile, the as-assembled MWCNTs/FeNi<sub>3</sub>/PANI-20//MWCNTs/FeNi<sub>3</sub>/PANI-20 symmetric supercapacitor also displayed a high energy density (9.1 Wh kg<sup>-1</sup> at a power density of 500 W kg<sup>-1</sup>) and an excellent electrochemical stability (80.9% capacitance retention after 2000 charge/discharge cycles). Therefore, the MWCNTs/FeNi<sub>3</sub>/PANI composites can be viewed as a sort of desirable electrode materials for supercapacitors.

**Funding information** This work was supported by the National Natural Science Foundation of China (Grant no. 61841504) and the Scientific Research Project of Heilongjiang Province (Grant no. JMRH201914).

## Compliance with ethical standards

**Conflict of interest** The authors declare that they have no conflict of interest.

## References

1. Guo YG, Hu JS, Wan LJ (2008) Nanostructured materials for electrochemical energy conversion and storage devices. *Adv Mater* 20: 2878–2887. <https://doi.org/10.1002/adma.200800627>
2. Simon P, Gogotsi Y (2008) Materials for electrochemical capacitors. *Nat Mater* 7:845–854. <https://doi.org/10.1038/nmat2297>
3. Zhang Y, Feng H, Wu X, Wang L, Zhang A, Xia T, Dong H, Li X, Zhang L (2009) Progress of electrochemical capacitor electrode materials: a review. *Int J Hydrog Energy* 34:4889–4899. <https://doi.org/10.1016/j.ijhydene.2009.04.005>
4. Singu BS, Yoon KR (2016) Porous 3D-β-nickel hydroxide microflowers for electrochemical supercapacitors. *J Ind Eng Chem* 33:374–380. <https://doi.org/10.1016/j.jiec.2015.10.036>
5. Min S, Zhao C, Chen G, Zhang Z, Qian X (2014) One-pot hydrothermal synthesis of 3D flower-like RGO/Co<sub>3</sub>O<sub>4</sub>/Ni(OH)<sub>2</sub> composite film on nickel foam for high-performance supercapacitors. *Electrochim Acta* 135:336–344. <https://doi.org/10.1016/j.electacta.2014.05.032>
6. Yan J, Fan ZJ, Sun W, Ning GQ, Wei T, Zhang Q, Zhang RF, Zhi LJ, Wei F (2012) Advanced asymmetric supercapacitors based on Ni(OH)<sub>2</sub>/graphene and porous graphene electrodes with high energy density. *Adv Funct Mater* 22:2632–2641. <https://doi.org/10.1002/adfm.201102839>

7. Kandalkar SG, Dhawale DS, Kim CK, Lokhande CD (2010) Chemical synthesis of cobalt oxide thin film electrode for supercapacitor application. *Synth Met* 160:1299–1302. <https://doi.org/10.1016/j.synthmet.2010.04.003>
8. Reddy ALM, Ramaprabhu S (2007) Nanocrystalline metal oxides dispersed multiwalled carbon nanotubes as supercapacitor electrodes. *J Phys Chem C* 111:7727–7734. <https://doi.org/10.1021/jp069006m>
9. Shaijumon MM, Rajalakshmi N, Ramaprabhu S (2006) Platinum/multiwalled carbon nanotubes-platinum/carbon composites as electrocatalysts for oxygen reduction reaction in proton exchange membrane fuel cell. *Appl Phys Lett* 88:253105. <https://doi.org/10.1063/1.2214139>
10. Sun M, Wang G, Li X, Cheng Q, Li C (2012) Interfacial synthesis and supercapacitive performance of hierarchical sulfonated carbon nanotubes/polyaniline nanocomposites. *Ind Eng Chem Res* 51:3981–3987. <https://doi.org/10.1021/ie202384u>
11. Mastragostino M, Arbizzani C, Soavi F (2001) Polymer-based supercapacitors. *J Power Sources* 812:97–98. [https://doi.org/10.1016/S0378-7753\(01\)00613-9](https://doi.org/10.1016/S0378-7753(01)00613-9)
12. Anderson MR, Mattes BR, Reiss H, Kaner RB (1991) Conjugated polymer films for gas separations. *Science* 252:1412–1415. <https://doi.org/10.1126/science.252.5011.1412>
13. Chiang JC, MacDiarmind AG (1986) ‘Polyaniline’: protonic and doping of the emeraldine form to the metallic regime. *Synth Met* 13:193–205. [https://doi.org/10.1016/0379-6779\(86\)90070-6](https://doi.org/10.1016/0379-6779(86)90070-6)
14. Kang ET, Neoh KG, Tan KL (1998) Polyaniline: a polymer with many interesting intrinsic redox states. *Prog Polym Sci* 23:277–324. [https://doi.org/10.1016/S0079-6700\(97\)00030-0](https://doi.org/10.1016/S0079-6700(97)00030-0)
15. Xu H, Li X, Wang G (2015) Polyaniline nanofibers with a high specific surface area and an improved pore structure for supercapacitors. *J Power Sources* 294:16–21. <https://doi.org/10.1016/j.jpowsour.2015.06.053>
16. Wang S, Ma L, Gan M, Fu S, Dai W, Zhou T (2015) Free-standing 3D graphene/polyaniline composite film electrodes for high-performance supercapacitors. *J Power Sources* 299:347–355. <https://doi.org/10.1016/j.jpowsour.2015.09.018>
17. Fan LZ, Hu YS, Maier J, Adelhelm P, Smarsly B, Antonietti M (2007) High electroactivity of polyaniline in supercapacitors by using a hierarchically porous carbon monolith as a support. *Adv Funct Mater* 17:3083–3087. <https://doi.org/10.1002/adfm.200700518>
18. Wang K, Meng Q, Zhang Y, Wei Z, Miao M (2013) High-performance two-ply yarn supercapacitors based on carbon nanotubes and polyaniline nanowire arrays. *Adv Mater* 25:1494–1498. <https://doi.org/10.1002/adma.201204598>
19. Zhu Z, Wang G, Sun M, Li X, Li C (2011) Fabrication and electrochemical characterization of polyaniline nanorods modified with sulfonated carbon nanotubes for supercapacitor applications. *Electrochim Acta* 56:1366–1372. <https://doi.org/10.1016/j.electacta.2010.10.070>
20. Zhang K, Hu H, Yao W, Ye C (2015) Flexible and all-solid-state supercapacitors with long-time stability constructed on PET/Au/polyaniline hybrid electrodes. *J Mater Chem A* 3:617–623. <https://doi.org/10.1039/c4ta05605a>
21. Jia J, Yu JC, Wang YXJ, Chan KM (2010) Magnetic nanochains of FeNi<sub>3</sub> prepared by a template-free microwave-hydrothermal method. *ACS Appl Mater Interfaces* 2:2579–2584. <https://doi.org/10.1021/am100410r>
22. Zhen L, Gong YX, Jiang JT, Shao WZ (2008) Electromagnetic properties of FeNi alloy nanoparticles prepared by hydrogen-thermal reduction method. *J Appl Phys* 104:34312–34321. <https://doi.org/10.1063/1.2959726>
23. Debski A, Gasior W, Moser Z, Major R (2010) Enthalpy of formation of intermetallic phases from the Au-Sn system. *J Alloys Compd* 491:173–177. <https://doi.org/10.1016/j.jallcom.2009.11.003>
24. Liu XG, Ou ZQ, Geng DY, Han Z, Jiang JJ, Liu W, Zhang ZD (2010) Influence of a graphite shell on the thermal and electromagnetic characteristics of FeNi nanoparticles. *Carbon* 48:891–897. <https://doi.org/10.1016/j.carbon.2009.11.011>
25. Zhao YW, Ni CY, Kruczynski D, Zhang XK, Xiao JQ (2004) Exchange-coupled soft magnetic FeNi-SiO<sub>2</sub> nanocomposite. *J Phys Chem B* 108:3691–3693. <https://doi.org/10.1021/jp037588r>
26. Cheng Y, Lu S, Zhang H, Varanasi CV, Liu J (2012) Synergistic effects from graphene and carbon nanotubes enable flexible and robust electrodes for high-performance supercapacitors. *Nano Lett* 12:4206–4211. <https://doi.org/10.1021/nl301804c>
27. Zhu C, Zhai J, Wen D, Dong S (2012) Graphene oxide/polypyrrole nanocomposites: one-step electrochemical doping, coating and synergistic effect for energy storage. *J Mater Chem* 22:6300–6306. <https://doi.org/10.1039/c2jm16699b>
28. Xu JJ, Wang K, Zu SZ, Han BH, Wei ZX (2010) Hierarchical nanocomposites of polyaniline arrays on graphene oxide sheets with synergistic effect for energy storage. *ACS Nano* 4:5019–5026. <https://doi.org/10.1021/nn1006539>
29. Zhang XW, Zhao DY, Luan DX, Bi CL (2016) Fabrication and mechanical properties of multiwalled carbon nanotube/nanonickel reinforced epoxy resin composites. *Appl Phys A Mater Sci Process* 122:1056–1058. <https://doi.org/10.1007/s00339-016-0597-3>
30. Bi CL, Zhao DY (2017) Enhancement in mechanical properties and conductivity of modified epoxy resin composites. *High Perform Polym* 1:1–14. <https://doi.org/10.1177/0954008317743308>
31. Kim M, Lee C, Jang J (2014) Fabrication of highly flexible, scalable, and high-performance supercapacitors using polyaniline/reduced graphene oxide film with enhanced electrical conductivity and crystallinity. *Adv Funct Mater* 24:2489–2499. <https://doi.org/10.1002/adfm.201303282>
32. Yu X, Li K, Zhou H, Wei S, Zhang C, Li X, Kuang Y (2015) Curly graphene nanosheets modified by nanoneedle-like manganese oxide for electrochemical capacitors. *RSC Adv* 5:88950–88957. <https://doi.org/10.1039/C5RA15529K>
33. Huang YP, Zhou JJ, Gao N, Yin ZX, Zhou HH, Yang XY, Kuang YF (2018) Synthesis of 3D reduced graphene oxide/unzipped carbon nanotubes/polyaniline composite for high-performance supercapacitors. *Electrochim Acta* 269:649–656. <https://doi.org/10.1016/j.electacta.2018.03.071>
34. Yuan B, Yu L, Sheng L, An K, Zhao X (2010) Comparison of electromagnetic interference shielding properties between single-wall carbon nanotube and graphene sheet/polyaniline composites. *J Phys D Appl Phys* 45:235108–235114. <https://doi.org/10.1088/0022-3727/45/23/235108>
35. Ghosh D, Giri S, Mandal A, Das CK (2013) Supercapacitor based on H<sup>+</sup> and Ni<sup>2+</sup> co-doped polyaniline-MWCNTs nanocomposite: synthesis and electrochemical characterization. *RSC Adv* 3:11676–11685. <https://doi.org/10.1039/c3ra40955d>
36. Chen SA, Lin LC (1995) Polyaniline doped by the new class of dopant, ionic salt: structure and properties. *Macromolecules* 28:1239–1245. <https://doi.org/10.1021/ma00108a062>
37. Lu K, Jiang RY, Gao X, Ma HY (2014) Fe<sub>3</sub>O<sub>4</sub>/carbon nanotubes/polyaniline ternary composites with synergistic effects for high performance supercapacitors. *RSC Adv* 4:52393–52401. <https://doi.org/10.1039/c4ra11088a>
38. Singu BS, Male U, Srinivasan P, Yoon KR (2017) Preparation and performance of polyaniline-multiwall carbon nanotubes-titanium dioxide ternary composite electrode material for supercapacitors. *J Ind Eng Chem* 49:82–87. <https://doi.org/10.1016/j.jiec.2017.01.010>
39. Ye TT, Kuang YF, Xie CJ, Huang ZY, Zhang CJ, Shan D, Zhou HH (2014) Enhanced performance by polyaniline/tailed carbon



- nanotubes composite as supercapacitor electrode material. *J Appl Polym Sci* 131:39971. <https://doi.org/10.1002/app.39971>
40. Ramana GV, Srikanth VV, Padya B, Jain PK (2014) Carbon nanotube-polyaniline nanotube core-shell structures for electrochemical applications. *Eur Polym J* 57:137–142. <https://doi.org/10.1016/j.eurpolymj.2014.05.018>
  41. Zhang J, Shu D, Zhang TR, Chen HY, Zhao HM, Wang YS, Sun ZJ, Tang SQ, Fang XM, Cao XF (2012) Capacitive properties of PANI/MnO<sub>2</sub> synthesized via simultaneous-oxidation route. *J Alloy Compd* 532:1–9. <https://doi.org/10.1016/j.jallcom.2012.04.006>
  42. Kim KS, Park SJ (2012) Synthesis and high electrochemical performance of polyaniline/MnO<sub>2</sub>-coated multi-walled carbon nanotube-based hybrid electrodes. *J Solid State Electrochem* 16: 2751–2758. <https://doi.org/10.1007/s10008-012-1694-7>
  43. Chen WY, Tao XQ, Wei DH, Wang HS, Yu Q, Li YC (2016) High-performance supercapacitor based on activated carbon-MnO<sub>2</sub>-polyaniline composite. *J Mater Sci Mater Electron* 27:1357–1362. <https://doi.org/10.1007/s10854-015-3897-z>
  44. Miao FJ, Shao CL, Li XH, Wang KX, Lu N, Liu Y (2016) Electrospun carbon nanofibers/carbon nanotubes/polyaniline ternary composites with enhanced electrochemical performance for flexible solid-state supercapacitors. *ACS Sustain Chem Eng* 4: 1689–1696. <https://doi.org/10.1021/acssuschemeng.5b01631>
  45. Singu BS, Srinivasan P, Yoon KR (2016) Emulsion polymerization method for polyaniline-multiwalled carbon nanotube nanocomposites as supercapacitor materials. *J Solid State Electrochem* 20:3447–3457. <https://doi.org/10.1007/s10008-016-3309-1>
  46. Miao FJ, Shao CL, Li XH, Lu N, Wang KX, Zhang X, Liu YC (2016) Polyaniline-coated electrospun carbon nanofibers with high mass loading and enhanced capacitive performance as freestanding electrodes for flexible solid-state supercapacitors. *Energy* 95:33–241. <https://doi.org/10.1016/j.energy.2015.12.013>
  47. Khosrozadeh A, Xing M, Wang Q (2015) A high-capacitance solid-state supercapacitor based on free-standing film of polyaniline and carbon particles. *Appl Energ* 153:87–93. <https://doi.org/10.1016/j.apenergy.2014.08.046>

**Publisher's note** Springer Nature remains neutral with regard to jurisdictional claims in published maps and institutional affiliations.